H/D isotope effects in high temperature proton conductors

Bonanos, Nikolaos; Huijser, A.; Poulsen, Finn Willy

Published in:
Solid State Ionics

Link to article, DOI:
10.1016/j.ssi.2015.03.028

Publication date:
2015

Document Version
Peer reviewed version

H/D Isotope Effects in High Temperature Proton Conductors

N. Bonanos, A. Huijser and F.W. Poulsen

Department of Energy Conversion and Storage, Technical University of Denmark
Risø Campus, P.O. Box 49, DK-4000 Roskilde, Denmark

nibo@dtu.dk

Abstract

The atomic mass ratio of *ca.* 2 between deuterium and hydrogen is the highest for any pair of stable isotopes and this results in significant and measurable H/D isotope effects in high temperature perovskite proton conductors containing these species. This paper discusses H/D isotope effects manifested in O–H/O–D vibration frequencies, the mobility of H^+/D^+ carriers, the kinetics of the electrochemical oxidation of H_2/D_2, the solubilities of H_2O/D_2O and, finally, the spontaneous electromotive force that appears across H_2/D_2 cells with proton conducting electrolytes. Comparable work on tritium-exchanged materials is also discussed. The usefulness of isotope effects in the study of high temperature proton conductors is highlighted.

1. Introduction: hydrogen and deuterium

The masses of hydrogen, deuterium and tritium are in the ratio 1/2/3, the largest for any set of isotopes.† Deuterium is stable, while tritium decays to ^{3}He with a half-life of 12.3 years releasing an electron. The mass difference does not noticeably affect the electronic structure of compounds formed by these species, but does affect their vibrational frequencies in the infrared, and also the vibrational entropy of the compounds. As a result, the physical and chemical properties of H/D compounds are affected, exemplified by the slightly higher vapour pressure of H_2O compared to D_2O‡ and a difference in the ionisation constants of the liquids [1]. Isotopic substitution also affects the length of hydrogen bonds [2]. The difference in Gibbs free energy of the reaction $2\ H_2 + O_2 \leftrightarrows 2\ H_2O$ and the corresponding one for D_2/D_2O is noticeable in an electrochemical cell. For example, the theoretical electromotive force (emf) of a cell with

† The masses of H, D and T are respectively 1.007825, 2.013553, and 3.01605 amu.
‡ For example, at 10°C, the vapour pressure of H_2O is 20% higher than that of D_2O.

D_2/D_2O (1%) *vs.* H_2/H_2O (1%) with an oxide ion conducting solid electrolyte can be calculated from thermodynamic data [3], in the temperature range 800 to 1200 K, resulting in eqn. (1):

$$E = -30.55 + 0.0128 \cdot T \quad (1)$$

where E is in mV and T in K. For the temperature range considered, the D_2/D_2O side is *negative*.

In high temperature proton conductors (HTPCs), the hydrogen species exist primarily as $OH^{\cdot}$ (Kröger-Vink notation) occupying oxide ion sites [4,5,6]. The hydrogen in the $OH^{\cdot}$ species is derived from water vapour via reaction (2). This reaction depends on the presence of oxide ion vacancies, which are usually introduced by doping with an element of lower valence. When the oxide is fully protonated, the $OH^{\cdot}$ concentration is determined by the doping level.

$$H_2O\,(g) + V_O^{\cdot\cdot} + O_O^{\times} \leftrightarrows 2\,OH_O^{\cdot} \quad (2)$$

A mechanism for proton incorporation that does not rely on water vapour is reaction (3) [7,8,9]. However, as it involves the creation of electronic defects, it is less favourable energetically. As demonstrated by a defect modelling study [10], reactions (2) and (3) are not mutually exclusive.

$$H_2\,(g) + 2\,O_O^{\times} \leftrightarrows 2\,OH_O^{\cdot} + 2\,e' \quad (3)$$

Isotope effects are the changes in the physical or chemical properties resulting from isotopic substitution. HTPCs offer several illustrations of such effects, such as changes in the concentration and ionic mobility of the protons and in the electrode kinetics of hydrogen oxidation. This work draws these effects together, in the hope of promoting better understanding of these diverse effects. Examples are provided from the subgroup of perovskite proton conductors [11]. The points raised apply to the class of HTPCs, but not necessarily to the class of low temperature proton conductors, where mostly vehicular transport mechanisms operate [12,13].

2. Isotope effects in perovskite proton conductors

Infra-red spectra

In the classical treatment of the O–H and O–D bonds as classical oscillators, the ratio of their vibration frequencies is determined by the reduced masses of the two systems, assuming that

the O atoms are unconstrained. For ^{16}O–^{1}H and ^{16}O–^{2}D, this ratio comes to $\sqrt{17/9}$, i.e. 1.374. For an H/D species attached to an infinite mass, the corresponding ratio would be $\sqrt{2}$, i.e. 1.414.

$$\frac{\omega_{O-H}}{\omega_{O-D}} = \sqrt{\frac{m^*_{O-D}}{m^*_{O-H}}} \tag{4}$$

where $$m^*_{O-H} = \frac{m_O m_H}{m_O + m_H} \tag{5}$$

and $$m^*_{O-D} = \frac{m_O m_D}{m_O + m_D} \tag{6}$$

Infra-red spectroscopic studies of D_2O vapour-exchanged perovskites and the perovskite-related structure $LiNbO_3$ showed a systematic shift in the O–D vibration peaks towards lower frequencies/wavenumbers [14,15,16]. Peaks associated with surface-bound protons were excluded from these studies. Fig. 1 shows the infra-red spectrum for the HTPC $La_{0.8}Sr_{0.2}ScO_{0.95}$ [12]. From the above works, the mean shift of sixteen peaks covering a total of nine compounds was found to be 1.343 ± 0.018, reasonably close to the value calculated based on the reduced mass.

Protonic conduction

The theories concerning the isotope effect and protonic conduction have been described in an important paper by Nowick and Vaysleyb [17]. The classical model predicts that the rate of a proton hopping in an oxide is proportional to the attempt frequency or O–H vibration frequency. Thus, the mobility of a proton should be larger than that of a deuteron by factor in the range 1.374 to 1.414, while the activation energies of the two species should be identical. These predictions do not agree with observations, therefore this model is discussed no further.

The so-called semi-classical treatment modifies the above model by considering the zero-point energy of the H/D species in the potential well in which they reside (Fig. 2). The zero-point energies are given by eqns (4, 5), in which ν_H, ν_D are vibrational frequencies.

$$E_{0,H} = \tfrac{1}{2} h\nu_H \tag{7}$$

$$E_{0,D} = \tfrac{1}{2} h\nu_D \tag{8}$$

The higher vibrational frequency of H results in a higher zero-point energy and, consequently, a lower energy barrier. Taking the mean of the frequencies reported in refs [14–16] results in a difference of 5.2 kJ mol^{-1} (0.054 eV), which should be reflected in the activation energies for migration. As for the pre-exponentials of the conductivity, these should be higher for protons than deuterons by a factor of 1.374 to 1.414, the latter value being usually quoted.

Nowick and co-workers assembled conductivity data on fifteen systems [15,16,17]. The average difference in activation energy was 4.3 kJ mol^{-1} (0.044 eV), 20% lower than that predicted by semi-classical theory. The discrepancy between observation and theory can be rationalised by recalling that the mechanism of proton transfer between oxygens is not one of simple hopping, but involves the vibrations and librations of the oxygen, as shown by Münch and Kreuer [18,19]. In effect, the barrier "seen" by the proton is modulated by the movements of the oxygen lattice. In contradiction of the semi-classical model, experimentally determined conductivity pre-exponentials are mostly higher for the D_2 exchanged HTPCs, in some cases by as much as 1.72.

The pre-exponential of the ionic conductivity may be described by the following equation [17]:

$$A = \frac{z\lambda^2 e^2 \nu_0 c_{eff}}{6\upsilon k} \tag{10}$$

where z is the number of jump directions

λ is the jump distance

e is the electronic charge

ν_0 is the vibration frequency

υ is the unit cell volume

k is the Boltzmann constant

c_{eff} is the effective concentration of carriers, allowing for association.

Inspection of equation (10) suggests that, apart from ν_0, c_{eff} is the only parameter with the freedom to vary significantly between H and D. Therefore, the inequalities $A_D > A_H$ and $\nu_{0,D} < \nu_{0,H}$, taken together, lead to the conclusion $c_{eff,D} > c_{eff,H}$, as pointed out previously by others [20].

Subsequent studies have confirmed the trends found by Nowick in D_2O-exchanged systems, with the significant exception of one study, which also involved tritium exchange [21]. In this study, $SrZr_{0.9}Yb_{0.1}O_{2.95}$ and $BaCe_{0.9}Yb_{0.1}O_{2.95}$ were investigated by impedance spectroscopy in atmospheres of $H_2/H_2O/Ar$, $D_2/D_2O/Ar$ and T_2/Ar.[§]. The impedance spectra were analysed to resolve the bulk properties, and these were subjected to an Arrhenius analysis. The activation energies followed the expected trend, increasing with isotope mass, except for one datum point, namely that of $BaCe_{0.9}Yb_{0.1}O_{2.95}$ in T_2/Ar (Fig. 3a). On the other hand, the pre-exponentials decreased with increasing isotope mass, in accordance with semi-classical theory, but contrary to trends documented by Nowick (Fig. 3b). The tritium anomaly in ΔH_m might have been explained by poor isotope exchange, considering that T_2/Ar was used in preference to T_2/T_2O, but the consistent trends observed in the pre-exponentials do not support this explanation.

Isotope effects in Electrode kinetics

The oxidation of hydrogen to protons involves steps of adsorption, dissociation, diffusion and charge transfer, all of which can be affected by isotopic substitution. Isotope effects have been observed in connection with hydrogen pumping [22] and with electrochemical hydrogen oxidation [23]. In the latter study, point contact electrodes of Ag and Ni were studied on the perovskite proton conductor $Sr_{0.995}Ce_{0.95}Y_{0.05}O_{2.975}$. Under conditions of anodic polarisation, mass transport limited currents were observed, whose dependence on P_{H_2} could be described by a power law. The reaction orders were 0.97 for Ni and 0.7 for Ag, suggesting that in the latter case the hydrogen atom was included in the rate determining step.

Fig. 4 shows the limiting currents in Arrhenius representation. Since these currents were thermally activated, they could not be ascribed to gas phase diffusion, but instead to bulk or surface diffusion, at least in the case of nickel. The phenomenological activation energies were higher for Ag than for Ni, and also higher for D_2 than for H_2, but did not follow the systematic pattern observed with the protonic conductivities.

Thermodynamic isotope effect

Tsidilkovski [24] considered the concentrations of H, D or T in an HTPC in equilibrium with H_2O, D_2O and T_2O vapour respectively. He pointed out that the difference in vibrational entropy between the vapour and solid phases influenced the Gibbs free energy of reaction (2)

§ T_2O was not included in the T_2/Ar atmosphere due to considerations of radiological safety.

for the three isotopes. Tsidilkovski demonstrated that, for equivalent hydration conditions, the concentration ratio [D]/[H] increased at low temperatures and low degrees of saturation; at temperatures of interest for HTPCs, this ratio exceeded the value of 2. Considering eqn. (10), this means that the conductivity pre-exponential for a D_2O-exchanged HTPC would exceed that of an H_2O exchanged one, even allowing for the lower attempt frequency of the D species.

Considering the relevance of the thermodynamic isotope effect to conduction mechanisms in HTPCs, scant attention has been given to its experimental study. We measured concentration isotherms of H and D in $Ba_3(Ca_{1.18}Nb_{1.82})O_{2-\delta}$ for H_2O and D_2O at 800 °C [25]. In Fig. 5, these are plotted against $P_{H_2O}^{½}$ and $P_{D_2O}^{½}$, which should give linear plots for low levels of saturation [26]. The results show significant differences between the isotherms for the two isotopes, although, contrary to our expectations, the lines do not pass through the origin. For the hydrogen isotherm, the results agree with those a previous study of the same compound [27]. Further work is needed to test these trends for other HTPCs materials and temperatures.

Spontaneous emf in H_2/D_2 cell

Matsumoto and co-workers have considered an electrochemical cell with HTPC electrolyte supplied with H_2 and D_2 on opposite sides. This results in the generation of an emf, for which the D_2 side is positive with respect to the H_2 side [28,29]. The emf arises because H^+ and D^+ migrate in opposite directions through the electrolyte, their two partial currents cancelling. Since the mobilities of the two species are different, but their partial currents the same, the resulting I·R drops must be different, generating to a net emf across the cell. A theoretical expression for the emf has been published earlier [29, 28]:

$$E_{th} = -\ln\left\{\frac{\left(2\mu_D^0 - \mu_{D_2}^0\right)}{2F} - \frac{\left(2\mu_H^0 - \mu_{H_2}^0\right)}{2F}\right\} + \frac{RT}{2F}\ln\left(\frac{p_{H_2}}{p_{D_2}}\frac{\gamma_D^2}{\gamma_H^2}\frac{u_D^2}{u_H^2}\right) \qquad (11)$$

where μ_i^0 are the standard chemical potentials of the species i, γ_i are the activity coefficients, u_i are the mobilities, the subscripts H_2/D_2 refer to the gaseous species and H/D to the species in the oxide, R, T and F have their usual meanings. Fig. 6 shows the second term of eqn. (11), for H_2/D_2 pressures of 1 atm, activity coefficients of unity and a mobility ratio of $\sqrt{2}$. Fig. 6 also includes experimental data obtained on such a cell with H_2/D_2 gases humidified at ambient temperature with H_2O/D_2O and a solid electrolyte of $CaZr_{0.9}In_{0.1}O_{2.95}$ (at the experimental conditions, $CaZr_{0.9}In_{0.1}O_{2.95}$ has a protonic transport number of close to unity). As pointed out

by Matsumoto [28], the magnitude of the observed H_2/D_2 cell emf indicates that the first term of eqn. (11) is negative, implying a greater solubility for D^+ than H^+. This is equivalent to the conclusions reached by Tsidilkovski regarding the thermodynamic isotope effect. Despite this, to our knowledge, the above two effects have not been treated in a unified manner.

It is remarkable that, for the same combination of atmospheres, H_2O/H_2O on one side and D_2/D_2O on the other, roughly similar emfs are generated, and that the sign of the emf depends on the conduction process in the electrolyte: negative for an oxide ion conductor (eqn. 1) and D positive for a proton conductor (eqn. 11). It is common for perovskite proton conductors to undergo a gradual transition from protonic to oxide ion conductivity at high temperatures, where the equilibrium of reaction (2) shifts to the left. Accordingly, the cell emf is expected to swing from positive to negative, passing through zero when the transport numbers of the two processes are equal.

Fig. 7 shows the response of two such cells for the perovskites $La_{0.7}Sr_{0.3}Sc_{0.8}Ti_{0.2}O_{2.95}$ [30] and $SrCe_{0.9}Y_{0.1}O_{2.95}$ [31], both of which are known to show such a transition. Thus, in principle, the H_2/D_2 cell emf serves as a diagnostic experiment of conduction mechanism, albeit a rather expensive one. It would be tempting to attempt to calibrate this method so that the curves in Fig. 7 could be converted to transport numbers, however this would be possible only if the polarisation resistances of the electrode processes for hydrogen/deuterium and for oxygen reactions were infinitely fast, an assumption that has been shown to be problematic [32].

Conclusions

The family of HTPCs show a wealth of effects when the hydrogen in the solids is replaced by deuterium. These affect the infra-red spectra, the transport properties, H_2/D_2 oxidation kinetics, solubilities of H_2O/D_2O and the behaviour of H_2/D_2 cells with proton conducting electrolytes. In our opinion, the following are the most important conclusions to be drawn from the above: 1) The concept of the classical harmonic oscillator is sufficient to explain the broad trends in the vibrational spectra, but not the transport properties, for which the semi-classical approach (or more advanced models) must be invoked. 3) The emf behaviour of H_2/D_2 electrochemical cells and the thermodynamic isotope effect both demonstrate a higher solubility of D_2O than H_2O in these systems, but these effects have not been unified into a single theory. 4) The sign of the emf of H_2/D_2 cells can be used to diagnose the mechanism of conduction in the electrolyte.

Acknowledgements

The authors acknowledge extensive contributions of their co-authors in previous publications, namely Mogens Mogensen, Marianne Glerup, Darja Kek, Charles Hatchwell and Henrik Bentzer. They are also grateful for valuable discussions with Hiroshige Matsumoto, Vladislav Tsidilkovski and Yurii Baikov. N. Bonanos thanks the FP7project MetProCell FCH-JU 277916 *Innovative Fabrication Routes and Materials for Metal and Anode Supported Proton Conducting Fuel Cells* for financial support in attending SSPC-17.

References

1. CRC Handbook 79th Edn., David R. Lide Editor-in chief, CRC Press (1998-99) p. 6.4.
2. A.R. Ubbelohde, K.J. Gallagher, Acid-base effects in hydrogen bonds in crystals, *Acta Crystallogr.* 8[2], 71–83 (1955).
3. M.W. Chase *et al*., JANAF Thermochemical Tables. Vol. 1-2, 3rd ed., New York, Amer. Inst. of Physics Inc. (1985).
4. T. Norby, M. Widerøe, R. Glöckner and Y. Larring, Hydrogen in oxides, *Dalton Transactions* **19**, 3012-3018 (2004).
5. K.-D. Kreuer, Proton-conducting oxides. *Annual Review of Materials Research* **33[1]**, 333-359 (2003).
6. N. Bonanos, Oxide-based protonic conductors, point defects and transport properties, *Solid State Ionics* **145**, 265-274 (2001).
7. I. Kosacki and H.L. Tuller, Mixed conductivity in $SrCe_{0.95}Yb_{0.05}O_3$ protonic conductors, *Solid State Ionics*, **80[3]**, 223-229 (1995).
8. S. Ricote, G. Caboche and O. Heintz, Synthesis and proton incorporation in $BaCe_{0.9-x}Zr_xY_{0.1}O_{3-\delta}$, *J. Appl. Electrochem.* ***39*[4]**, 553-557 (2009).
9. Y.M. Baikov, The chemical state and the mobility of hydrogen in oxide–hydroxide solids, *Solid State Ionics* **97[1]**, 471-476 (1997).
10. N. Bonanos and F.W. Poulsen, Considerations of defect equilibria in high temperature proton conducting cerates, *J. Mater. Chem*. **9**, 431-434 (1999).
11. N. Bonanos, "Perovskite Proton Conductor", in *Encyclopedia of Applied Electrochemistry*, Eds. R. Savinell, K. Ota and G. Kreysa, Springer-Verlag, Berlin, Heidelberg, pp. 1514-1520 (2014).
12. A. Potier, "The hydrogen bond and parameters favouring proton mobility in solids", in *Proton Conductors: Solids, membranes and gels – materials and devices*, Ed. P. Colomban, Cambridge University Press (1992), p. 6.
13. P. Colomban, *Proton Conductors, Solids, membranes, gels – materials and devices*, Cambridge University Press (1992).
14. M. Glerup, F.W. Poulsen and R.W. Berg, Vibrational spectroscopy on protons and deuterons in proton conducting perovskites, *Solid State Ionics* **148**, 83 (2002).

15. W.-K. Lee, A.S. Nowick and L.A. Boatner, Protonic conduction in acceptor-doped $KTaO_3$ crystals, *Solid State Ionics* **18**, 989-993 (1986).
16. T. Scherban, Y.M. Baikov and E.K. Shalkova, H^+/D^+ isotope effect in Y-doped $BaCeO_3$ crystals, *Solid State Ionics* **66**, 159-164 (1993).
17. A.S. Nowick and A.V. Vaysleyb, Isotope effect and proton hopping in high-temperature protonic conductors, *Solid State Ionics*, **97**, 17-26 (1997).
18. W. Münch, G. Seifert, K.-D. Kreuer and J. Maier. A quantum molecular dynamics study of proton conduction phenomena in $BaCeO_3$. *Solid State Ionics* **86**, 647-652 (1996).
19. W. Münch, K.-D. Kreuer, G. Seifert and J. Maier, Proton diffusion in perovskites: comparison between $BaCeO_3$, $BaZrO_3$, $SrTiO_3$ and $CaTiO_3$ using quantum molecular dynamics, *Solid State Ionics* **136**, 183-189 (2000).
20. R.C.T. Slade and N. Singh, Generation of charge carriers and H/D isotope effect in proton conducting doped barium cerate ceramics, J. Mater. Chem. **1[3]**, 441-445 (1991).
21. R. Mukundan, E. L. Brosha, S.A. Birdsell, A.L. Costello, F.H. Garzon and R.S.Willms, Tritium conductivity and isotope effect in proton conducting perovskites, *J. Electrochem. Soc.*, **146[6]**, 2184-2187 (1999).
22. T. Hibino, K. Mizutani and H. Iwahara, H/D isotope effect on electrochemical pumps of hydrogen and water vapor using a proton conductive solid electrolyte *J. Electrochem. Soc*, **140**, 2588 (1993).
23. D. Kek and N. Bonanos, Electrochemical H/D isotope effects at metal/perovskite proton conductor interfaces, *Solid State Ionics* **125[1-4]**, 345-353 (1999).
24. V. I. Tsidilkovski, Thermodynamic isotope effect H/D/T in proton-conducting oxides, *Solid State Ionics* **162**, 47-53 (2003).
25. J.M. Huijser, Isotope effects in proton conducting oxides, M.Sc. project report, Materials Research Department, Risø National Laboratory, Roskilde, Denmark (2003).
26. A.S. Nowick, Yang Du, High-temperature protonic conductors with perovskite-related structures, *Solid State Ionics* **77**, 137-146 (1995).
27. F. Krug and T. Schober, The high-temperature proton conductor $Ba_3(Ca_{1.18}Nb_{1.82})O_{9-\alpha}$: thermogravimetry of the water uptake, *Solid State Ionics*, ***92*[3-4]**, 297-302 (1996).
28. H. Matsumoto, K. Takeguchi & H. Iwahara, Electromotive force of hydrogen isotope cell with a high temperature proton conducting solid electrolyte $CaZr_{0.90}In_{0.10}O_{3-\alpha}$, *J. Electrochem. Soc.* **146[4]** 1486-1491 (1999).
29. H. Matsumoto, H. Hayashi, T. Shimura, H. Iwahara and T. Yogo, Electrochemical hydrogen isotope sensing via the high-temperature proton conductor $CaZr_{0.90}In_{0.10}O_{3-\alpha}$, *Solid State Ionics* **161**, 93–103 (2003).
30. C. Hatchwell, N. Bonanos & M. Mogensen, The role of dopant concentration, A-site deficiency and processing on the electrical properties of strontium- and titanium-doped lantha num scandate, *Solid State Ionics* **167**, 349-354 (2004).
31. H. Bentzer, Development of Materials for Hydrogen Permeable Membranes, Ph.D. Thesis, Technical University of Denmark (2010).
32. H.K. Bentzer, N. Bonanos & J.W. Phair, EMF measurements on mixed protonic/electronic conductors for hydrogen membrane applications, *Solid State Ionics* **181**[3-4], 249-255 (2010).

Figure Captions

Fig. 1 Infra-red spectrum of HTPC $La_{0.8}Sr_{0.2}ScO_{3-d}$ treated in N_2/D_2O. Peaks for O—H and O—D are clearly resolved [14]. Note the presence of shoulders on the low wavenumber side of the peaks.

Fig. 2 Semi-classical picture of proton and deuteron in a finite potential well adapted from ref. [17]. The different zero-point energies of the two species results in an activation energy for D^+ migration that is 5.2 kJ/mol higher than for that for H^+.

Fig. 3 Arrhenius conductivity parameters in HTPCs exchanged with the three isotopes of hydrogen, based on data in ref. [21]. The activation energies increase with isotope mass, except for one point for $BaCe_{0.9}Yb_{0.1}O_{2.95}$, while the pre-exponentials decrease, contrary to expectations from ref. [17].

Fig. 4 Temperature dependence of anodic limiting currents in the oxidation of hydrogen/deuterium [23]. The study was performed using Ni and Ag point contact electrodes in $N_2/1\%H_2$ and $N_2/1\%H_2$.

Fig. 5 Concentration isotherms for [H] and [D] in $Ba_3(Ca_{1.18}Nb_{1.82})O_{2-\delta}$ at different partial pressures of H_2O and D_2O, at 800 °C [25], together with results for [H] from another study [27]. Plotting the concentrations versus $(PH_2O)^{½}$ linearizes the isotherm, such that, for low vapour pressure, the slope is $\sqrt{M_b K_w/2}$ [26].

Fig. 6 Second term of eq. (8) for the theoretical emf of a D_2/H_2 electrochemical cell plotted against temperature and the experimental emf obtained using the solid electrolyte $CaZr_{0.9}In_{0.1}O_{2.95}$ [28]. The lower line is the theoretical emf for the corresponding cell with oxide ion conductor (eqn. 8).

Fig. 7 Emf of D_2/H_2 electrochemical cells for the perovskites $La_{0.7}Sr_{0.3}Sc_{0.8}Ti_{0.2}O_{2.95}$, described in ref. [30], and $SrCe_{0.9}Y_{0.1}O_{2.95}$ [31]. With increasing temperature, both systems display a transition from protonic to oxide ion conduction, concomitant with the cell emf approaching zero.

Figure(s)

Click here to download high resolution image

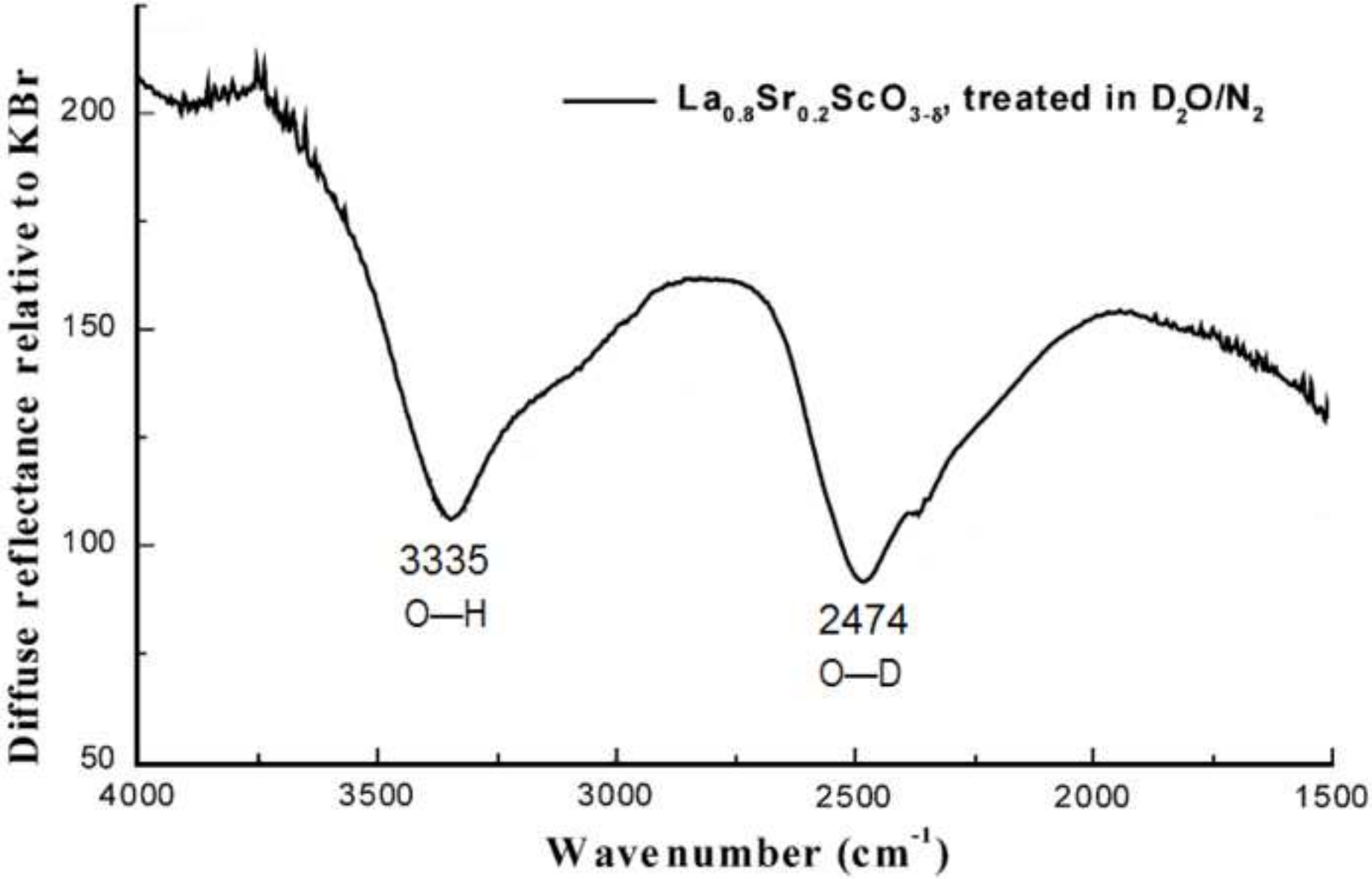

Figure(s)

Click here to download high resolution image

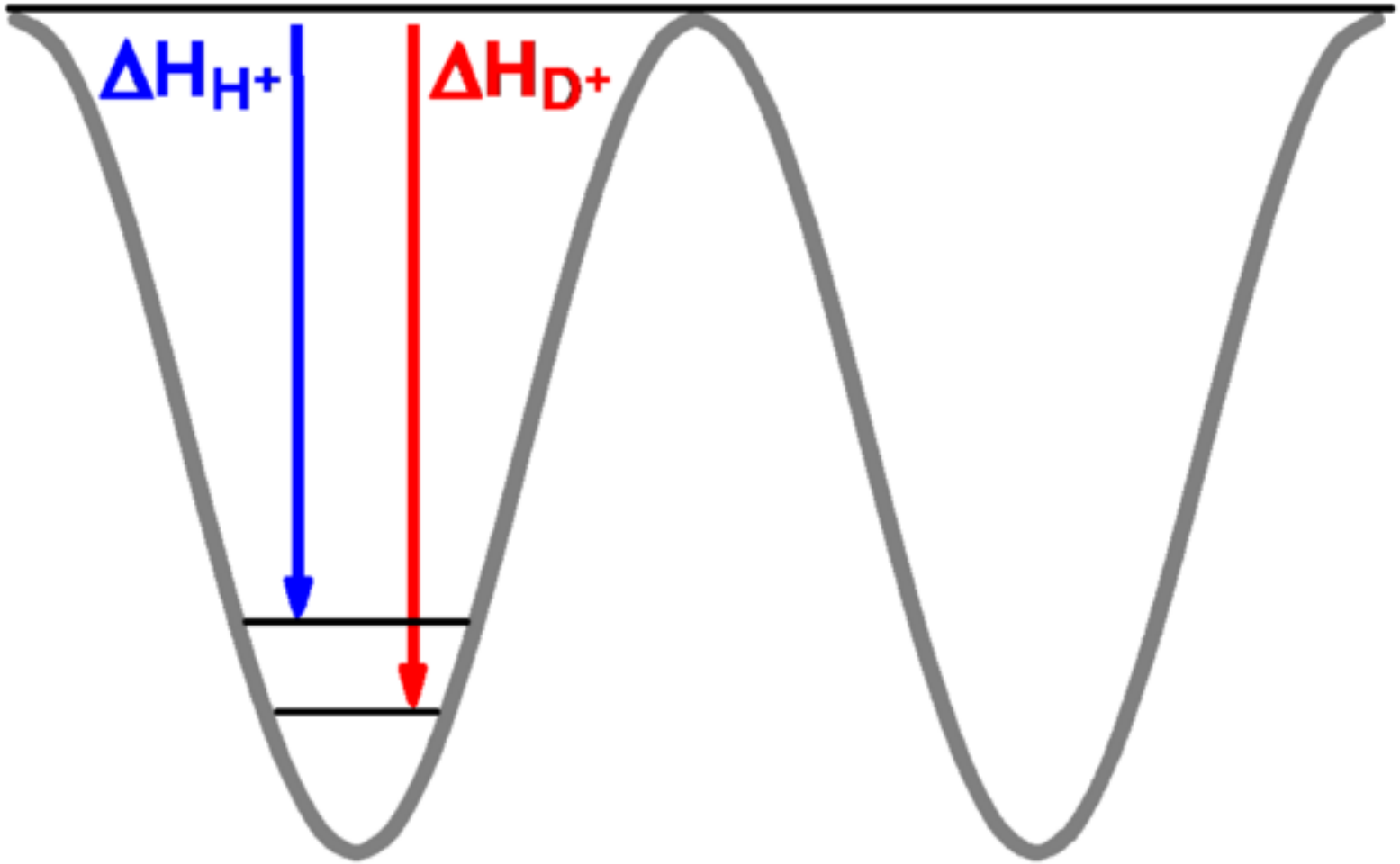

Figure(s)

Click here to download high resolution image

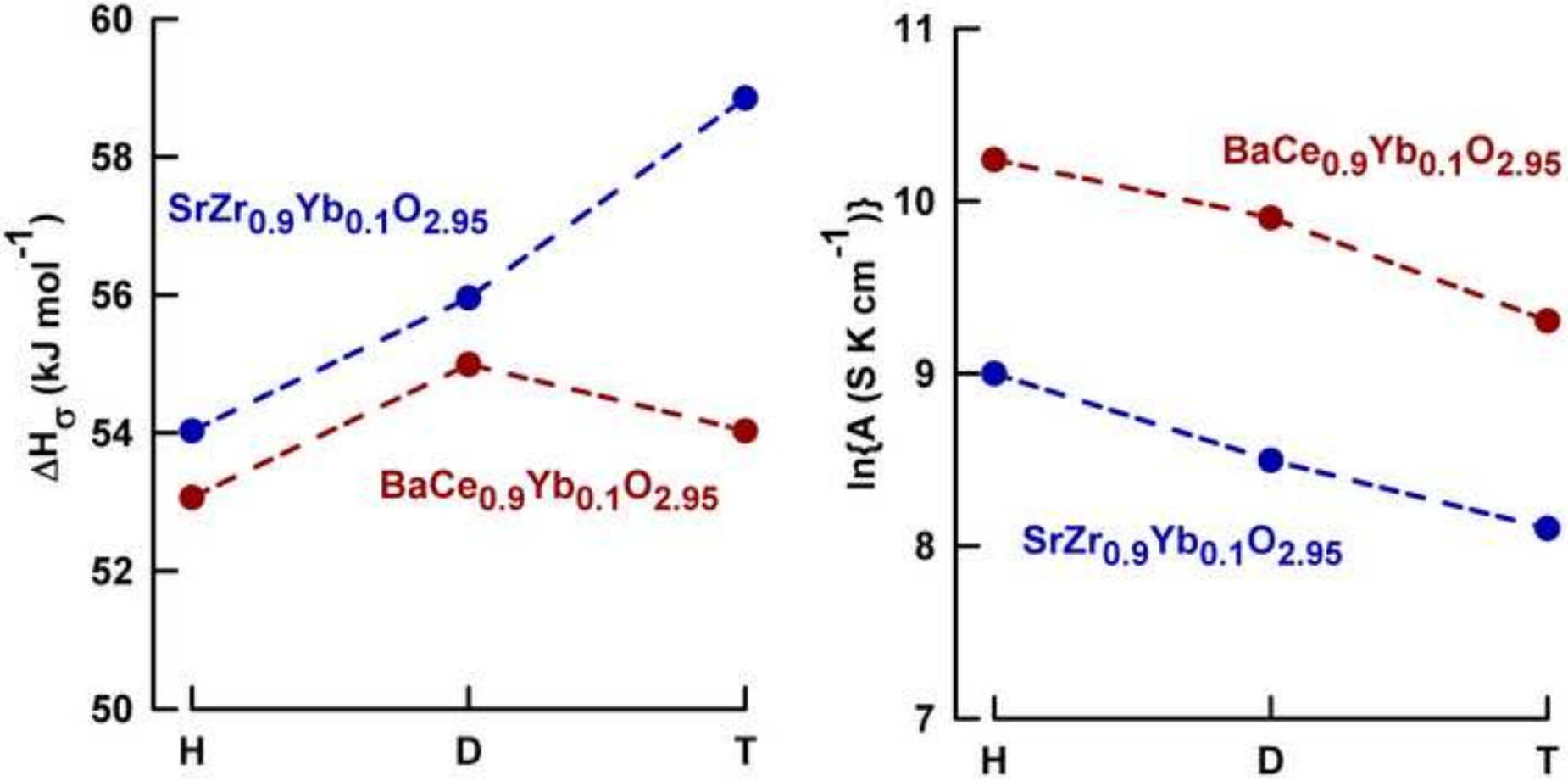

Figure(s)
Click here to download high resolution image

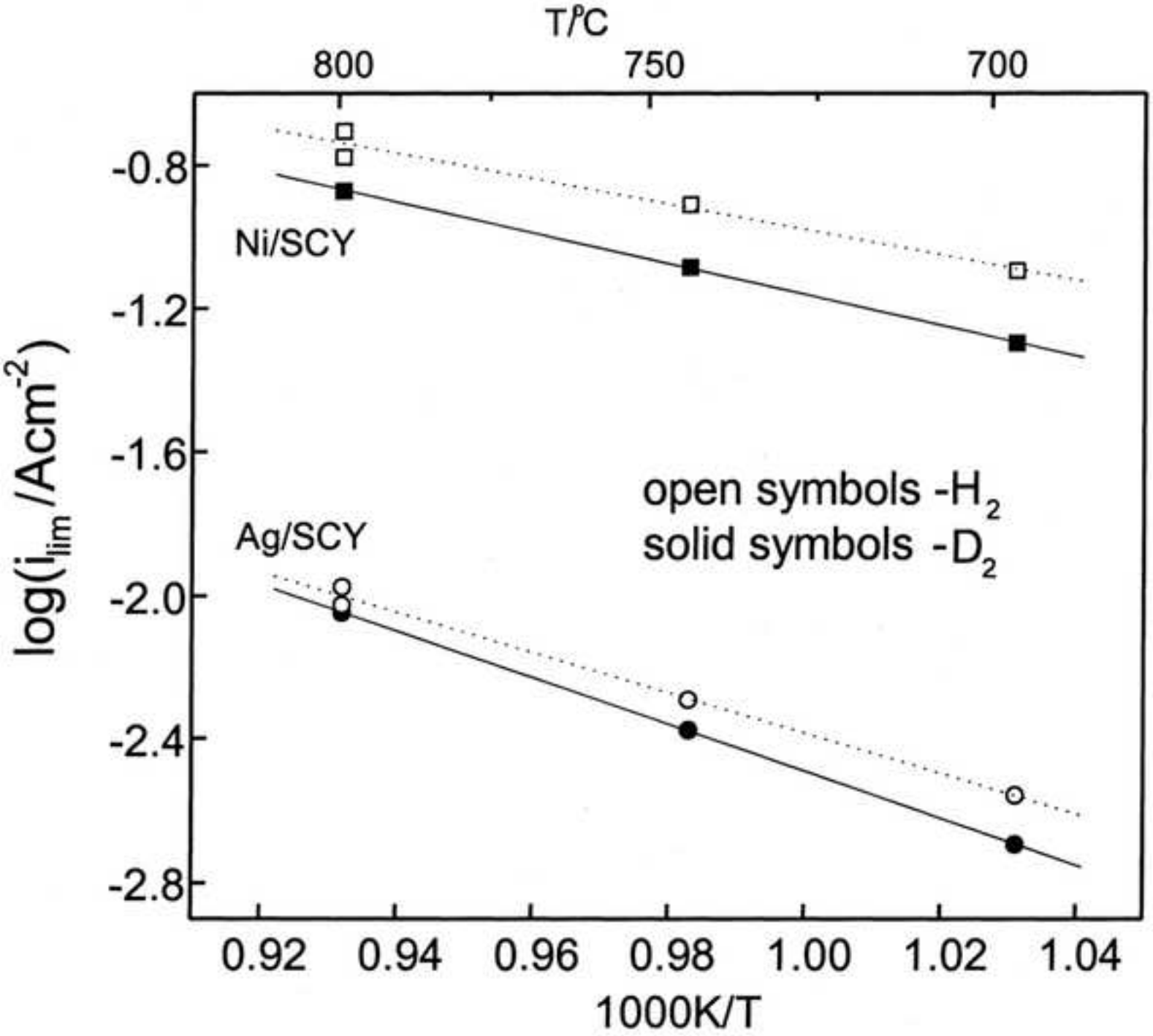

Figure(s)

Click here to download high resolution image

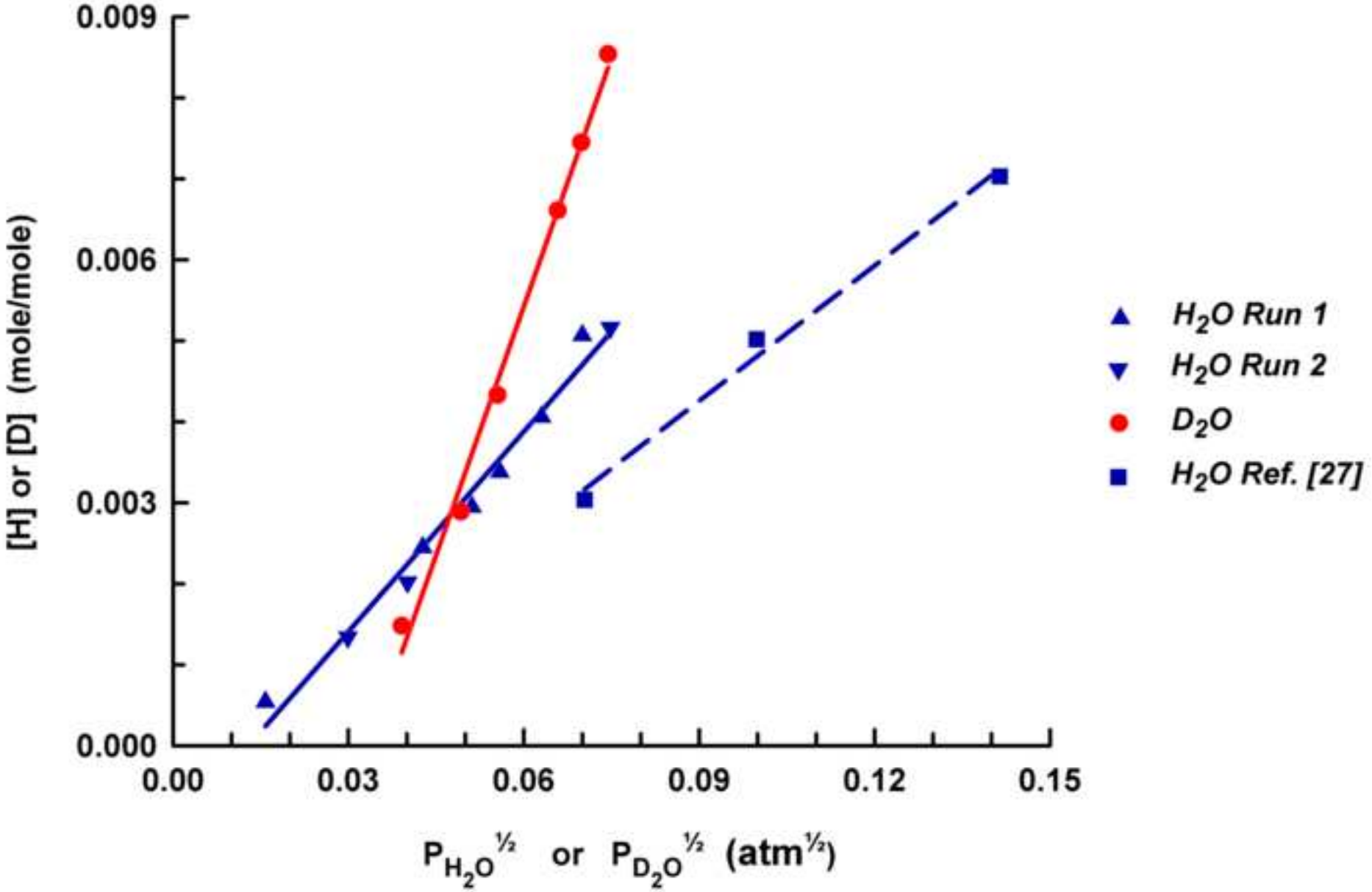

Figure(s)
Click here to download high resolution image

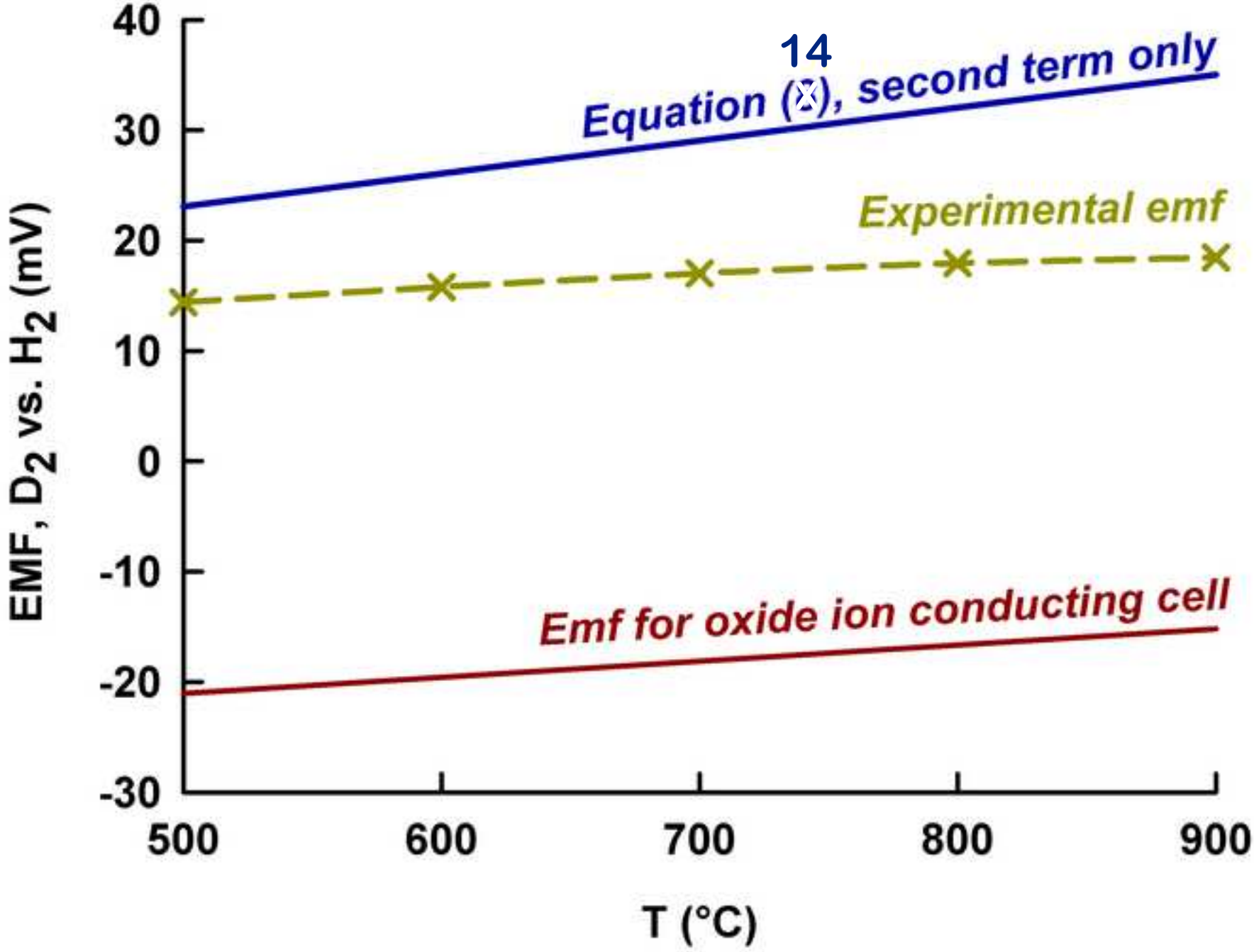

Figure(s)

Click here to download high resolution image